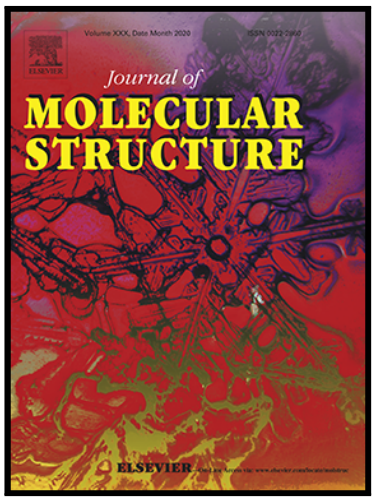

Magnetic Hydrochar nanocomposite obtained from sunflower husk: A potential material for environmental remediation

Aura Alejandra Burbano Patiño , Verónica Leticia Lassalle , María Fernanda Horst

PII: S0022-2860(21)00642-6
DOI: https://doi.org/10.1016/j.molstruc.2021.130509
Reference: MOLSTR 130509

To appear in: *Journal of Molecular Structure*

Received date: 14 January 2021
Revised date: 31 March 2021
Accepted date: 10 April 2021

Please cite this article as: Aura Alejandra Burbano Patiño , Verónica Leticia Lassalle , María Fernanda Horst , Magnetic Hydrochar nanocomposite obtained from sunflower husk: A potential material for environmental remediation, *Journal of Molecular Structure* (2021), doi: https://doi.org/10.1016/j.molstruc.2021.130509

Magnetic Hydrochar nanocomposite obtained from sunflower husk: A potential material for environmental remediation

Aura Alejandra Burbano Patiño, Verónica Leticia Lassalle, María Fernanda Horst*

INQUISUR, Departamento de Química, Universidad Nacional del Sur (UNS)-CONICET, Av. Alem 1253, 8000 Bahía Blanca, Argentina

Highlights

- Novel magnetic hydrochar from sunflower husk is successfully synthesized.
- Coulombic interactions are the main mechanism of interact between magnetite nanoparticles and hydrochar.
- Magnetic hydrochar has good stability at short times in real water sample.

Graphical abstract

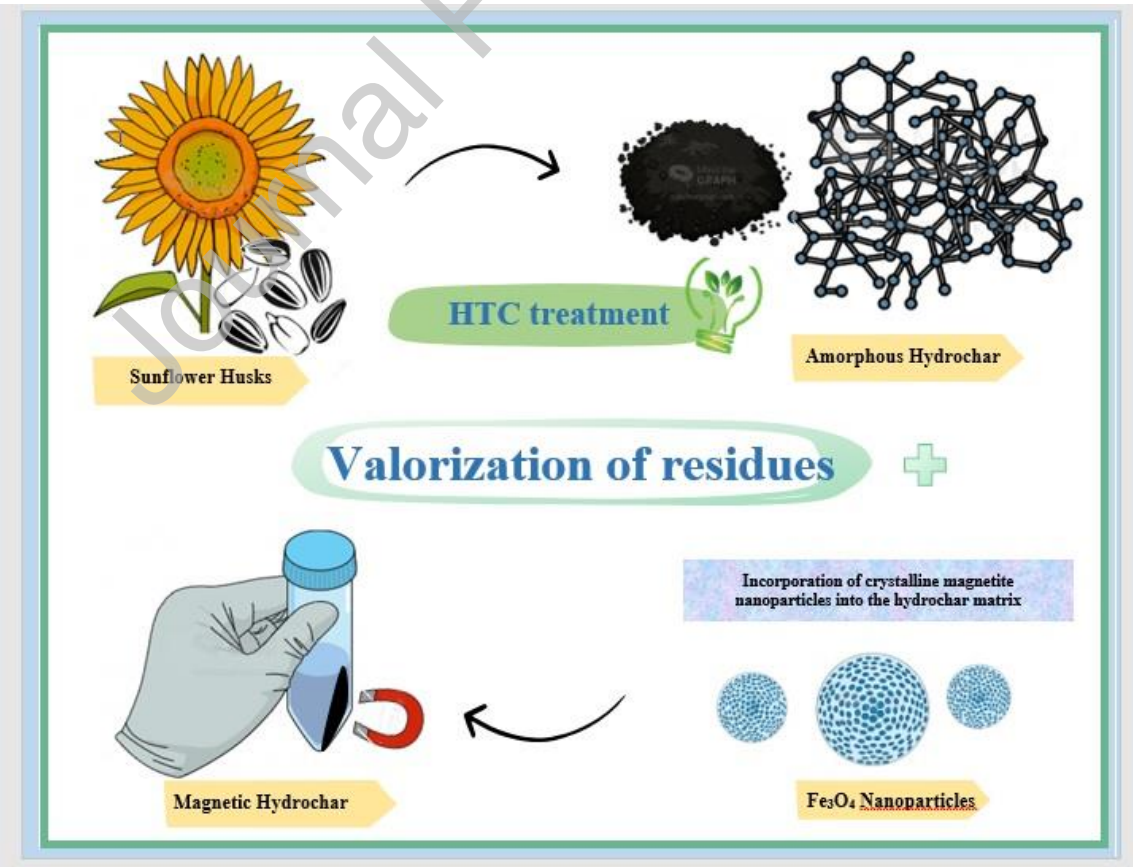

Abstract

A novel magnetic hydrochar composed of nanosized magnetite (Fe3O4) particles supported on a hydrochar matrix was synthesized via hydrothermal carbonization of sunflower husk, employing phosphoric acid as the activating agent. An exhaustive characterization of the hydrochars and the magnetic hydrochar was undertaken to identify, mainly, the mechanism by which the iron oxide nanoparticles interact with the hydrochar matrix. The magnetic hydrochar exhibited superparamagnetic properties with a saturation magnetization of 55,21 emu/g. BET surface area and pore diameter of the magnetic hydrochar were found to be 55.25 m^2/g and 10,49 nm respectively which are in accordance with mesoporous materials. Fourier transform infrared spectroscopy and z potential characterization suggest that the main mechanisms of interaction between the magnetite nanoparticles and the hydrochar matrix were coulombic ones, where carboxyl and hydroxyl oxygen-containing functional groups of the hydrochar were more likely to interact with the iron oxide nanoparticles.

Keywords: sunflower husk, magnetic hydrochar, hydrothermal carbonization, environmental remediation.

Corresponding author: PhD. María Fernanda Horst; mfhorst@uns.edu.ar

1. Introduction

Nowadays, the valorization of biomass is becoming of great importance since it's a way to reuse and recycle materials (that are produced in large amounts in different areas including agriculture and livestock) and converting them into more functional products. As a case of point, thermochemical conversion of biomass (pyrolysis, gasification, or hydrothermal carbonization) into hydrochars or biochars is an efficient approach where the biomass is treated at different conditions of temperature, pressure, residence time, biomass to water ratio, and pH of the

substrate that will lead to materials with particular physicochemical properties [1–3]. Hydrochars seem to appear as prospective materials that can be employed in numerous fields some of which are nanoelectronics, catalysis, optics, biosensors, environmental remediation, energy, hydrogen storage, drug transport, magnetic resonance imaging, and cancer diagnosis [4–8]

Hydrochars are produced via Hydrothermal Carbonization (HTC) which is an effective technically-attractive thermochemical exothermic process that converts biomass into rich carbonaceous materials. Commonly, it operates at relatively low temperatures (≈100-300 °C) compared to pyrolysis and autogenous pressure [9]. The temperature should be above 100 °C since at this first range, chemical reactions take place including hydrolysis, dehydration, decarboxylation, condensation, polymerization, and aromatization [10]. Despite hydrochars having interesting physicochemical properties, their implementation as adsorbents [11,12], is compromised because of their subsequent separation from the aqueous media. This stage commonly requires complex procedures involving centrifugation or filtration that leads to mass of adsorbents loss as well as possible contamination of the aqueous media. On account of this, the possibility of modifying the HC by incorporating magnetic moieties such as magnetite or maghemite on its surface has been investigated as a viable solution. The presence of these inorganic oxides would be useful due to their magnetic properties because they could be removed from the media by an external magnetic field. Besides, in some cases the existence of iron oxides offers a synergy regarding the adsorption capacity for certain pollutants, thus enhancing the removal efficiency of the adsorbents [13,14].

Sunflower Husk (SFH) is a biomass waste generated in the industrial process of production of sunflower oil where the seed is directly used and the husk is a residue that may be combusted and serve in thermal energy [15]. This biomass represents one of the most important agro-industrial wastes in Argentina, particularly in Buenos Aires province. Argentina cultivates annually around 1.35 million ha to produce 3.7 million ha of sunflower seed [16,17]. In turn, the industry oil company produces just over 1.25 million Mg year-1 of sunflower oil, leaving a shell

residue of 600000 Mg year-1 [16]. The literature reports that SFH is an organic residue with an important amount of lignin, cellulose, and other elements such as K, Ca, Mg y S in minor proportions [18].

Some works reported the synthesis of composites including HTC and magnetite particles. Kazazk et al. [19] studied a magnetic hydrochar prepared by the HTC method which produced a porous structure hydrochar (Vtotal= 0.071 cm3/g and BET surface area=23 m2/g) that contributed to the adsorption of Pb (II) at pH 5 within 120 minutes of equilibrium time. Shuqing Guo et al. [20] studied an HTC process that was carried out using lawn grass as the feedstock and exploring different temperatures (200-240 °C) and times (30-180 min) [20]. On the other hand, Moonis Ali Khan et al. [21] reported a nitrogen-doped magnetic hydrochar developed from sugarcane bagasse and used as an adsorbent of transition heavy metals. The characterization results reveal that the material was mesoporous (BET surface area: 62.5 m^2/g) and that the main surface functional groups were oxygen and nitrogen from FTIR and XPS analysis. The batch adsorption experiments showed 75-80% of percent removal efficiencies. Another study from Hasan Sayğılı et. al [22], includes iron hydrochar produced from an industrial waste product. Characterization results (XRF, SEM-EDX, XRD, FTIR, BET, and VSM) showed a successful impregnation of iron into the hydrochar. Furthermore, the material was applied in the adsorption of methylene blue and methyl orange where the maximum adsorption capacity was 11 and 8.9 mg/g respectively.

Recent studies devoted to magnetic hydrochar synthesis from different biomass wastes have shown that these types of materials provide an efficient and promising way to solve water remediation problems by adsorption due to their structural, chemical, and morphological characteristics. Their magnetic property makes them even more interesting to separate from an aqueous media giving the possibility of reuse. Additionally, the different feedstocks used to prepare hydrochars showed an excellent alternative to a circular economy where high-volume wastes are converted into valuable products. Besides, HTC has shown in previous studies

several advantages over conventional thermochemical methods as no prior drying is requested and the high quality of the char is suitable for water treatment applications [23–25].

This work aims to prepare hydrochar from sunflower husk (SHF) by hydrothermal carbonization method, as a raw material for the synthesis of magnetic hydrochar. The objectives include analyzing the hydrothermal conditions such as residence time and temperature, which give rise to hydrochars with different characteristics to determine the optimum one. All the materials were characterized by BET, FTIR, DRX, TGA, and TEM. Besides, chemical analysis, DLS, and zeta potential were employed. For MHC, magnetic properties were studied by VSM. Finally, the possible mechanisms of interaction between hydrochar and the iron oxide nanoparticles were studied.

2. Materials and Methods

2.1 Materials

In this study, sunflower husk (SHF) was used as the feedstock. Ferrous sulfate heptahydrate ($FeSO_4.7H_2O$) and ferric chloride hexahydrate ($FeCl_3.6H_2O$) of analytical grade were used for the synthesis of magnetite nanoparticles and were purchased from Cicarelli Laboratory (Argentina), ammonium hydroxide (NH_4OH) was provided by Anedra Laboratory (Argentina), Phosphoric acid (H_3PO_4) at 50% was utilized as the activating agent.

2.1.1 Pretreatment of sunflower husk (SFH)

SFH was washed up with tap water to remove dust and dirt. Secondly, the husks were washed all over again employing bidistilled water and repeated the procedure until the washing water was clean enough. Finally, the husks were dried in an oven at 40 °C for 5 days. The dried SFH was crushed using a blender and sieved by a 50 mesh Sigma Aldrich sieve (297 µm) until and homogeneous pore size and conserved in plastic jars.

2.1.2 Preparation of activated hydrochar

In this first step, an amount of SFH (2 g) was added into a flask containing 50 mL of the activating agent phosphoric acid (H_3PO_4) 50%. The mixture was kept under stirring for 5

minutes. Following, the resultant mixture was added into a 100 mL Teflon-lined stainless-steel reactor and then transferred to an oven and heated at 150 ºC. The influence of treatment time was explored by using: 3 h (HC1), 6 h (HC2), and 24 h (HC3). After cooling down until ambient temperature, the hydrochar was washed and rinsed under vacuum filtration until pH 6 and subsequently dried at 40 ºC. Residence time is the average length of time that the hydrothermal reaction remains in a reservoir, in other words, the time that the reactor had been left in the oven.

2.1.3 Synthesis of magnetic hydrochar

The synthesis of magnetic hydrochar was conducted by in situ co-precipitation of magnetite nanoparticles into the hydrochar matrix, following an adaptation of previously reported works [26,27]. In a typical procedure, 1.6 g of Fe^{3+} and 0.6 g of Fe^{2+} 2:1 were initially stirred for 3 hours in presence of 0.5 g of HC at room temperature. The iron oxide:hydrochar ratio was selected of 1:1. Then, 6 mL of NH_4OH 28-30% was added dropwise (1 mL/min). Later on, this mixture was added to a Teflon-lined stainless-steel reactor which was transferred to the oven and left for 3 hours at 150 ºC (this selected residence time was taken into account by hydrochar characterization that will be discussed in another section). Finally, the black solid (MHC) was purified by washing with distilled water to get rid of the impurities by using an external magnetic field and dried at 40 ºC.

Scheme 1 summarizes a graphical view of the pathways for the experimental procedure.

Scheme 1

2.1.4 Stability test

The stability of the materials was performed by incubating them in bidistilled and real water samples using 100 mg of material in 100 mL of bidistilled/real water under vigorous stirring. Then, aliquots were taken every 2 hours (approximately) for 72 hours. Each aliquot was filtered and measured at 215-240 nm by spectroscopy UV-visible using Agilent 8453 equipment [28].

2.1.5 Characterization techniques

Fourier Transform Infrared (FTIR) spectroscopy of HC and MHC has been recorded on a Thermo Scientific Nicolet iS50 FT-IR: Thermo Scientific Nicolet iS50 NIR module with Integrating Sphere in the frequency range 4000–400 cm^{-1} for the characterization of surface functional groups. The surface physical morphology of HC and MHC was examined by Transmission Electron Microscopy (TEM). Malvern Zetasizer Nano ZS90 was employed to measure the Z potential (ξ) and the average hydrodynamic diameter of particles by dynamic light scattering (DLS). Elemental analysis using an Exeter analytical CE-440 under optimal equipment operating conditions was carried out. The method uncertainty is ± 0.40% for each of the specific elements. For these measurements, the observed error was ± 0.76. The detection limit (LD) is 1 µg for each of the specified elements. Thermal stability analysis of hydrochars was performed in a TA Q500 instrument at room temperature up to 500 °C at 10 °C/min under air atmosphere. Atomic absorption spectroscopy was used to determine mg Fe/mg present in MHC. For this purpose, an amount of the material was weighed and disaggregated in hydrochloric acid 10%. Then aliquots of this dissolution were measured in the ABC Avanta 932 spectrometer.

N_2 adsorption-desorption isotherms of carbonaceous organic materials took place using a Quantachrome Autosorb iQ surface analyzer equipment with its control software and data analysis (ASiQwin 6.0). The samples were pretreated with heat and vacuum at 200 ° C and 1x10-3 Torr for 48 hours in a 9 mm glass cell. The absorbed volume data ranged from $7x10^{-2}$ to 750 Torr (P / P0 = $7x10^{-5}$ to 1) of N_2 was analyzed using Brunauer - Emmett - Teller (BET) theory taking relative pressure points according to the Rouquerol et al. [29], to determine the specific surface area. For the determination of the distribution of pore diameter and pore volume in the requested ranges, DFT and Barrett-Joyner-Halenda (BJH) methods were used by adjusting the experimental data for each measurement.

Magnetization curves, expressing specific magnetization (M) as a function of applied magnetic field (H) at room temperature, were obtained using a vibrating sample magnetometer (VSM) LakeShore 7404 operated with maximum applied fields μ0Hmax = 1.8 T.

3. Results and discussion

3.1 Hydrochar and Sunflower husk characterization

3.1.1 FTIR characterization

FTIR spectra of all materials were recorded to identify functional groups present in hydrochar, and SHF. Figure 1 depicts the FTIR spectra showing the main typical peaks of this biomass residue. The broadband located at 3100 to 3700 cm^{-1} is associated with the stretching vibration of O-H (in hydroxyl or carboxyl groups) and water adsorbed on the surface [30]. A band at 2900 cm^{-1} can be attributed to C-H aliphatic stretching vibration which is more evident in hydrochars and less intense in the SFH spectrum [30]. Around 1700 cm^{-1} a signal appears a vibration related to the C=O functional group that almost disappears in SFH demonstrating that components of SFH degraded and simultaneously underwent a polymerization reaction [20]. The band at 1612 cm^{-1} was ascribed to the asymmetric stretching vibration of aromatic C=C [19]. Furthermore, hydrochar obtained from sunflower husk was activated with H_3PO_4, the band between 900 and 1200 cm^{-1} may be attributed to the presence of phosphorus species in the samples [31].

Figure 1

3.1.2 Elemental analysis

Chemical analysis of hydrochars and sunflower husk was conducted using elemental analysis to estimate their composition. The reached data are summarized in Table 1. Sunflower husk has a relatively high carbon content. After hydrothermal carbonization, hydrochars 1, 2, and 3 increased their carbon content from 46.57 to 68.40% as the residence time increases from 3 to 24 hours. More complete carbonization of the products can be achieved by operating at longer

residence times. Furthermore, oxygen and hydrogen decrease as the residence time increases. They were transformed into gas through a dehydration reaction [12]. The dehydration reaction carbonized biomass by lowering H/C and O/C. Some other chemical reactions and mechanisms are involved in HTC but according to the evidence from available literature substantial hydrolysis of cellulose and lignin occur above 200 °C [32]. These results are congruous with some previous investigations where hydrochar was obtained from corn cob residual. Those data showed that carbon composition increased with increasing residence time, whereas oxygen and hydrogen decreased [33].

Table 1

3.1.3 Zeta potential and hydrodynamic diameter

Table 2 lists the data corresponding to the hydrodynamic diameter and zeta potential of SFH and HC1,2 and 3.

The zeta potential value and sign are related to the surface charge of the particle materials. As it could be observed the zeta potential of all materials are negative in aqueous dispersions (pH around to 5.5). These results were consistent with those found for other hydrochar in the literature [34]. Moreover, as will be discussed in the section below, the z potential of SFH and HC are negative from 3 to 8 pH values. This is indicative that functional groups with a negative charge are mainly exposed to the surface of SFH and HC materials. This was supported by FTIR characterization where it was confirmed the presence of e.g. – COOH (1700 cm^{-1}), – OH (3100-3700 cm^{-1}). Other authors found negative zeta potential values in biochars produced from straws of canola, corn, soybean, and peanut at different pyrolysis temperatures [34].

As reflected in Table 2, as the residence time increases from HC1 to HC2, the hydrodynamic diameter decreases (enhance their stability in an aqueous solution). It was studied that the residence time has a similar effect compared with the temperature in hydrothermal carbonization methods [10]. It was demonstrated that a long residence time has an effect on the

polymerization of fragments solved in the liquid phase, so this led to the formation of secondary hydrochar and consequently to form microspheres particles [35].

Table 2

3.1.4 Adsorption and desorption of N_2 isotherms

BET surface area, pore volume, and pore width results are shown in Table 3. The N_2 adsorption-desorption isotherms form part of supplementary material. The adsorption-desorption isotherms of hydrochars belong to VI isotherm type (that are characteristic of mesoporous materials) and H4 hysteresis loop. In this study it was determined that the analyzed samples recorded low values of adsorption volume of N_2 (~ 150 cm^3 / g - 23 cm^3 / g), according to the values of surface area and total pore volume found for the materials (HC1> HC2> HC3 = SFH sorted in decreasing values). The pore size distribution shows that these are mesoporous materials with little macropore contribution [36]. The micropore contribution is negligible in the HC1 to HC2 samples while in SFH it appears more substantial than in the previous samples, which was observed at the peak at 2 nm in the BJH model and 1.5 nm in the adjustment distribution by the method DFT (data not shown). In most of the studies that are related to hydrochars, isotherms are type I (as IUPAC classification) governed by the presence of micropores [37]. However, this depends on different conditions, such as the utilized feedstock, the temperature range and residence time. As can be seen in table 2, surface area and pore volume increase for HC1 and HC2 compared to the raw SFH. A difference was appreciable when residence time was increased to 24 hs, a diminished in these parameters was observed. Moreover, as residence time increases from HC1 to HC3, BET surface area and pore volume decrease. These results demonstrated that the hydrochar properties are dependent on hydrothermal process conditions such as residence time. Similar results were obtained by other authors using oil palm shells [38]. From the results, it could be said that a higher surface area and pore volume could be obtained with lower temperature, and residence time of the hydrothermal conditions process. These results were confirmed in a recent study where the authors analyzed the role of hydrochar properties on the porosity of hydrochar-based porous carbon materials [39].

From BET surface area, pore volume, and pore width, HC1 was the selected material to synthesize the magnetic hydrochar (MHC). This selection was done taking into account that the surface parameters were considered convenient for the potential application of the material as an adsorbent in water remediation. From hereinafter, it'll be called HC.

Table 3

3.2 Magnetic hydrochar characterization

3.2.1 FTIR characterization

In **Figure 2,** the MHC sample exhibits a vibration at 585 cm^{-1} related to the stretching vibration of the Fe-O bond corresponding to iron oxide [40]. As it can be seen in the FTIR spectrum of HC, there are functional groups such as OH^- and $COOH^-$ that vibrate approximately at 3400 and 1600 cm^{-1} that could participate in the interaction with magnetite. In comparison, most of the vibrations that are present in the HC disappear in the MHC suggesting that magnetite nanoparticles are integrated into the surface of the hydrochar probably by a physical force such as coulomb interaction [41]. Besides, in the MHC spectrum, O-H vibration has shifted to a lower wavenumber and the C=O present in $COOH^-$ has disappeared. This indicates that these two groups are more likely to interact with magnetite nanoparticles. Similar results were obtained in similar materials, for example, a magnetic hydrochar from nanocellulose [30] and magnetic porous carbon from waste hydrochar [42].

Figure 2

3.2.2 Structural analysis

Figure 3 displays the XRD patterns obtained from the hydrochar and compares them with the one corresponding to SFH. MHC diffractogram sharp peaks at 2θ values characteristic of magnetite crystalline structure are observed. The crystalline planes of magnetite are evidenced at 18°, 30°, 35°, 42°, 53°, 57°, and 62° that are ascribable to (111), (220), (311), (400), (422), (511) and (440). These results were compared with standard reference patterns and measurements to identify the ferromagnetic phase in MHC. This is consistent with the reference

magnetite with tab number 19-629 [43]. It has an inverse spinel structure with face-centered cubic lattice and where Fe^{3+} and Fe^{2+} occupied octahedral and tetrahedral sites [44]. Hence, this demonstrates the successful incorporation of magnetite on the hydrochar. On the other hand, an intense broadband can be seen at 2θ: 23°, which according to the literature indicates the presence of an amorphous phase that in this case is ascribed to the hydrochar [45]. Similar studies have shown that this broadband is related to disordered carbons such as hydrochars and biochars with a high carbon content that appear between 20° and 30° [46,47].

Figure 3

3.2.3 Morphological analysis

TEM images of the magnetic hydrochar at different magnifications are shown in Figure 4. It could be seen that magnetite particles are distributed in the hydrochar matrix that appears as colorless support (fig4 c and d). The particles are well dispersed in the HC matrix showing in some cases agglomerates of particles. From TEM micrographs it could be suggested that magnetic particles were stabilized by the HC. As it was already mentioned from FTIR characterizations, the disappearance of some characteristic peaks of HC when magnetite particles were incorporated suggested that inorganic moieties should be integrated into the HC matrix, and this could be observed by TEM images. The magnetite particles appear as spheres that are the predominant shape. The particle size reaches values from 9 to 24 nm, approximately (fig.4 b). These results are consistent with previous studies that have worked with magnetic bio and hydrochars and have shown a good dispersion of Fe_3O_4 on the surface of the biochar with a particle size of approximately 10-20 nm [30,48].

For comparison TEM images of HC and magnetite particles could be observed in Figures 4a and b. The hydrochar that was exposed to hydrothermal carbonization at 150 °C for 3 hours, has cellulose fibers appearance as seen in figure 4a. After magnetite incorporation, the hydrochar looked a little different from the previously obtained. This is due to the hydrochar undergoing another 3 hours of heating at 150 °C, which means more residence time, leads to a different morphological structure from fibers to a smooth appearance due to further decomposition of

carbonaceous material. Similar images were observed by other authors in hydrochar magnetic materials [42]. Moreover, the presence of magnetic nanoparticles in the hydrochar matrix showed aggregate nanoparticles into the hydrochar matrix. Similar results were observed by other authors in biocompatible magnetic composite obtained from egg white biomass [49].

Figure 4

Besides, BET analysis could be conducted to have information about the surface area and the morphological structure of the material. The BET measurements yielded values of 55.52 m2/g. This result is consistent with a mesoporous material without the presence of macroporous as well as microporous. The pore diameter predicted was estimated at 10.49 nm. Comparing the results obtained for the HC matrix, the BET surface area was diminished when the magnetite nanoparticles were incorporated into the hydrochar. Nevertheless, an increase in the pore diameter was observed. These results could be attributed to the temperature time which was exposed the hydrochar when the iron oxides moieties were incorporated by the second hydrothermal carbonization. This reinforces the results observed by TEM and which was described before. Similar results were observed by other authors [50]. In this study, magnetic hydrochar was synthesized by hydrothermal carbonization evaluating different carbonization temperatures. The authors observed by BET characterization that the surface area of magnetic carbon composites decreased with increasing the production temperature of hydrochar.

3.2.4 Magnetic characterization

The VSM measurements were conducted to characterize the magnetic property of magnetic hydrochar. As it can be seen in figure 5, the magnetic hydrochar demonstrated to have superparamagnetic properties since the magnetization curve shows a saturation magnetization value of 55.21 emu/g in the order of which obtained for bulk magnetite (roughly 80 emu/g) in our previous researches [51] and a coercivity of 0.164 oe.

Figure 5

Other authors observed a saturation magnetization value of 13.6 to 16.3 emu/g for a hydrochar magnetic material [50]. The authors attributed the differences to the different content on Fe_2O_3 particles. For instance, Hasan Sayğılı has reported a synthesis of magnetic hydrochar by using grape pulp as bio-waste material and it was reported a saturation magnetization and coercivity of 2 emu/g and 15 Oe, respectively [22].

3.2.5 Zeta potential, hydrodynamic diameter, and surface charge as a function of pH

Table 2 shows the hydrodynamic diameter and zeta potential of HC and also MHC values. The hydrodynamic diameter value obtained for MHC was notably smaller (670 nm) than the corresponding one for HC (1 µm). This result was consistent with those observed for naked magnetite nanoparticles (532 nm). These results are consistent with those observed by TEM micrographs where magnetite particles have a size of around 20 nm. It is important to mention that for hydrodynamic measurements, the values are considered the hydrated particle in the suspension. These results were similar to those obtained for the particle size distribution of orange peel hydrochar and Fe-orange peel hydrochar [52].

In aqueous media, the z potential of MHC compared with HC, registered higher negative values. For instance, at pH 5.5, z potential of HC was 6.16 and -20.3 for MHC. The presence of negative surface charge on HC and also in MHC was attributed to the functional groups present in this type of hydrochar where the feedstock was from lignocellulosic biomass, such as carboxyl and hydroxyl. MHC experienced a second "hydrothermal carbonization" causing the hydrochar to undergo once more a series of reactions as hydrolysis and dehydration which have affected the cellulose, hemicellulose, and lignin structure. So, the consequence of these series of reactions have led to exposed negative acidic and basic surface functional groups [10]. Previous studies have demonstrated that functional groups such as carboxyl and hydroxyl present in the hydrochar play an important role in its inherent negative charge [53].

The z potential as a function of pH was studied for raw magnetite nanoparticles, HC and MHC, and data are depicted in Figure 6. The analysis was conducted by adjusting the ionic strength with two electrolytes, NaCl and KNO_3 0.01M. In both electrolytes, the z potential of the HC and

MHC are negative across the pH range of 3 to 9. This was ascribed as it was already mentioned to dissociation of biomass structure so exhibited hydroxyl and carboxyl groups on the surface. Similar results were obtained by Wang et al. [54] for magnetic greigite/biochar. As pH increases, zeta potential decreases for both materials and both electrolytes. This behavior was due to as pH increases, deprotonation process takes place. Furthermore, MHC reached a higher magnitude of negative zeta potential when compared with HC caused by its magnetic component [32]. It is evident from the development of MHC zeta potential that it has achieved a different material when it was incorporated into magnetite nanoparticles. From the data arising from the material's characterization, it is possible to suggest that the HC and the magnetite might interact by physical forces such as electrostatic interaction as a result of the difference between zeta potentials. These results are consistent with previous researches found in the literature. For example, Yanfei Li et al. synthesized a magnetic activated carbon whose zeta potential was found to be negative and increased the negative charge as increasing the pH, showing the importance of O-containing functional groups [55].

Figure 6

3.2.6 Thermogravimetric analysis

Figure 7 shows the thermal degradation curves of HC and MHC. Firstly, as it could be seen from the weight loss curves, the incorporation of iron oxide particles contributes to increasing the decomposition temperature of the HC. Below 200 °C, both samples showed a weight loss of 3.036% associated with the presence of interstitial water present in both materials. In HC, the first main weight loss from after 200 °C is correlated to the decomposition of biopolymers present in the HC such as fractions of cellulose, hemicellulose, and lignin [56]. The devolatilization of organic occurs in the range from 250 °C until 550 °C [57]. As it could be observed, the weight loss in MHC is considerably lower compared with HC, which proposes that the presence of Fe_3O_4 in HC increases the thermal stability [58]. These results are congruous with prior research of magnetic hydrochars where the first weight loss was related to the water moieties present in the surface of particles in the material. The loss after 200 °C can

be associated with the decomposition of organic substances involving small molecules such as oxygen-containing functional groups -OH, -COOH, and -CO. Beyond 500 °C, weight loss is associated with the decomposition of both inorganic and organic residues [59,60].

Moreover, the thermogravimetric measurement of magnetite nanoparticles synthesized by hydrothermal methodology is not shown since the authors have been synthesized magnetite nanoparticles by co-precipitation methodology and analyzed by TG characterization [27]. It analyzed the thermogravimetric measurements of magnetite particles obtained by HT methodology [61]. In this study, the authors found closed similar TG curves for magnetite nanoparticles synthesized by HT with those obtained in our previous studies. As it was described in both research a total mass loss was around 5% until almost 800 K, attributable to water content. Both magnetite nanoparticles synthesized by the two different techniques demonstrated almost identical thermogravimetric curves, that was the reason for which it is not presented in the TG curves in this study.

Figure 7

The iron content was analyzed on MHC. The analysis was conducted by measuring the Fe content by triplicate using absorption atomic spectroscopy. From the results, it could be said that the Fe content was around 50% of the total mass (48.52 mg Fe/100 mg of material). So, the results are following the nominal ratio used for the synthesis of 1:1 for Mag:HC.

3.2.7 Stability test of MHC

The stability test was conducted in bidistilled water and real water samples. This assay was important taking into account the potential application of biochar magnetic material as an adsorbent of pollutants in aqueous media. The tests were conducted by incubating MHC material in bidistilled water (pH around 6.0) and real underground water sample (pH around 8.0) collected from route 35, km 15 of the region of Bahía Blanca, southwest of Buenos Aires province from Argentina.

According to our knowledge, there have been studies where the biochars could release dissolved organic carbon (DOC) when it was applied in soils and water, and DOC could modify the physicochemical properties of these media [62]. The different fractions of DOC generate a signal in the UV-visible region (at around 254 nm) that may be detected by UV-visible spectrometry signal [63]. DOC compositions were analyzed by Fourier transform ion cyclotron, gas chromatography coupled with mass spectrometer and FTIR, among others [64,65], and its compositions were in general small organic compounds composed of phenolic, acid, and bio-oil compounds, among others which depends on the origin of the biomass used to produce the biochar.

Figure 8 depicts the UV-vis spectra of supernatant arising from the incubation of MHC on bidistilled (fig.8a) and real water (fig.8b) samples, respectively. As it could be observed both spectra presented an absorbance band between 215 to 240 nm at the different times of incubation. This behavior could be attributable to organic dissolved compounds [63]. The absorbance values around 220 to 240 nm demonstrates quite different absorbance values, being higher absorbances for bidistilled water than in real water samples. Although an increase in the absorbance values was observed when the incubation time is longer, it was registered at 3 and 6 hs of the assay, an absence or little absorbance value at this wavelength. So, it could be said that the material had not shown notable organic matter leaching during the first experiment. Despite these results, the absorbance values in bi-distilled water were higher in comparison with those raised by the stability test in the real water sample. It could appreciate a diminution of the absorbance value when MHC was incubated in the real water sample, meanwhile, when the material was put in contact with bidistilled water, a high increase of the absorbance at 220/240 nm could be observed. Moreover, the supernatant of the assays demonstrated a dark brown color for bidistilled water incubation, meanwhile, in real water samples, the solutions had light-yellow or almost transparent color. From these results, it could be said that the MHC material has less DOC release when it's suspended in a real water sample than when it is employed in bidistilled water. Similar results were obtained by Liu et al. [63] analyzing DOC extracted

solutions in water, acid and basic media. The authors observed that the extracted solutions had from light-yellow to dark-yellow color.

Otherwise, it was studied in the research group other magnetic materials, such as biopolymer magnetic nanocomposites, where it was observed that at 220 nm a signal is attributable to Fe leaching from the materials [66]. So, it could be said that there is an overlapping of both signals from the DOC and Fe leaching and contribute in the same manner to the instability of the MHC.

Figure 8

3.2.8 Mechanism of formation of MHC

From FTIR, zeta potential results, and TEM micrographs it could be possible to propose a possible mechanism by which the hydrochar interacts with magnetite nanoparticles. Figure 9 represents the possible mechanism by the principal functional groups of hydrochar that have interacted with magnetite nanoparticles to form the magnetic hydrochar material. It could be observed that carboxyl and hydroxyl were the probable functional groups from hydrochar that interact with magnetite nanoparticles. This suggestion could be reinforced with the results obtained by FTIR characterization. As it was observed by FTIR analysis that the bands corresponding to carboxyl groups from hydrochar disappeared when iron oxides were incorporated, so it would be one of the responsible interactions that could be raised in the formation of MHC. The interaction could be by the formation of C – O – Fe. This interaction was also observed by other authors in the synthesis of magnetic hydrochar from cellulose [30]. Besides, in figure 9 it could be observed a photograph of the magnetic behavior of MHC when an external magnetic field was applied by an Nd –imam, as a qualitatively magnetic property.

Figure 9

4. Conclusion and outlook

"In this research the valorization of agro-industrial waste from Argentina was studied for the development of novel adsorbent material. From characterization data, it was observed that in MHC material the possible main mechanism by which the magnetite nanoparticles interact with

hydrochar is by coulombic interactions between carboxyl and hydroxyl functional groups from hydrochar and iron oxides nanoparticles. Based on the material characterization it is possible to suggest that the MHC synthesized in this work could be used as potential adsorbent for environmental remediation, especially as an adsorbent of emergent pollutants. The practical application of this material will be presented in a separate contribution."

Declaration of interests

The authors declare that they have no known competing financial interests or personal relationships that could have appeared to influence the work reported in this paper.

Acknowledges

The authors acknowledge the financial support of ANCyPT (PICT 2018-03476), CONICET and Universidad Nacional del Sur (PGI 24/ZQ09).

The authors acknowledge the valuable contribution of PhD. Marcela Fernandez Van Raap and the Institute of Physics from La Plata, Argentina (IFLP-UNLP-CONICET) for their collaboration in the magnetic measurements.

References

[1] Z. Zhang, Z. Zhu, B. Shen, L. Liu, Insights into biochar and hydrochar production and applications: A review, Energy. 171 (2019) 581–598. https://doi.org/10.1016/j.energy.2019.01.035.

[2] S. Zhang, X. Zhu, S. Zhou, H. Shang, J. Luo, D.C.W. Tsang, Hydrothermal carbonization for hydrochar production and its application, Elsevier Inc., 2018. https://doi.org/10.1016/B978-0-12-811729-3.00015-7.

[3] S. Suranani, V.R. Goli, Fuel Particle Size Effect on Performance of Fluidized Bed Combustor Firing Ground Nutshells, Int. J. Chem. Eng. Appl. 3 (2012) 147–151. https://doi.org/10.7763/ijcea.2012.v3.176.

[4] Committee, Roadmap for Bioenergy and Biobased Products in the United States, October. (2007).

[5] M.A. Khan, A.A. Alqadami, S.M. Wabaidur, M.R. Siddiqui, B.H. Jeon, S.A. Alshareef, Z.A. Alothman, A.E. Hamedelniel, Oil industry waste based non-magnetic and magnetic hydrochar to sequester potentially toxic post-transition metal ions from water, J. Hazard. Mater. 400 (2020) 123247. https://doi.org/10.1016/j.jhazmat.2020.123247.

[6] S. Joseph, G. Saianand, M.R. Benzigar, K. Ramadass, G. Singh, A.I. Gopalan, J.H. Yang, T. Mori, A.H. Al-Muhtaseb, J. Yi, A. Vinu, Recent Advances in Functionalized

Nanoporous Carbons Derived from Waste Resources and Their Applications in Energy and Environment, Adv. Sustain. Syst. 5 (2021) 1–30. https://doi.org/10.1002/adsu.202000169.

[7] S. Mandal, S. Pu, S. Adhikari, H. Ma, D.H. Kim, Y. Bai, D. Hou, Progress and future prospects in biochar composites: Application and reflection in the soil environment, Crit. Rev. Environ. Sci. Technol. 51 (2021) 219–271. https://doi.org/10.1080/10643389.2020.1713030.

[8] T. Xie, K.R. Reddy, C. Wang, E. Yargicoglu, K. Spokas, Characteristics and applications of biochar for environmental remediation: A review, Crit. Rev. Environ. Sci. Technol. 45 (2015) 939–969. https://doi.org/10.1080/10643389.2014.924180.

[9] D. Basso, F. Patuzzi, D. Castello, M. Baratieri, E.C. Rada, E. Weiss-Hortala, L. Fiori, Agro-industrial waste to solid biofuel through hydrothermal carbonization, Waste Manag. 47 (2016) 114–121. https://doi.org/10.1016/j.wasman.2015.05.013.

[10] T. Wang, Y. Zhai, Y. Zhu, C. Li, G. Zeng, A review of the hydrothermal carbonization of biomass waste for hydrochar formation: Process conditions, fundamentals, and physicochemical properties, Renew. Sustain. Energy Rev. 90 (2018) 223–247. https://doi.org/10.1016/j.rser.2018.03.071.

[11] M. Puccini, E. Stefanelli, A.L. Tasca, S. Vitolo, Pollutant removal from gaseous and aqueous phases using hydrochar-based activated carbon, Chem. Eng. Trans. 67 (2018) 637–642. https://doi.org/10.3303/CET1867107.

[12] B. Li, J. Guo, K. Lv, J. Fan, Adsorption of methylene blue and Cd(II) onto maleylated modified hydrochar from water, Environ. Pollut. 254 (2019) 113014. https://doi.org/10.1016/j.envpol.2019.113014.

[13] D.W. Cho, K. Yoon, E.E. Kwon, J.K. Biswas, H. Song, Fabrication of magnetic biochar as a treatment medium for As(V) via pyrolysis of FeCl3-pretreated spent coffee ground, Environ. Pollut. 229 (2017) 942–949. https://doi.org/10.1016/j.envpol.2017.07.079.

[14] Y. Yi, Z. Huang, B. Lu, J. Xian, E.P. Tsang, W. Cheng, J. Fang, Z. Fang, Magnetic biochar for environmental remediation: A review, Bioresour. Technol. (2019) 122468. https://doi.org/10.1016/j.biortech.2019.122468.

[15] G. Maj, P. Krzaczek, A. Kuranc, W. Piekarski, Energy Properties of Sunflower Seed Husk as Industrial Extrusion Residue, Agric. Eng. 21 (2017) 77–84. https://doi.org/10.1515/agriceng-2017-0008.

[16] J.C. Vallejos, M.D.L. Echeverría, UTILIZACIÓN DE CÁSCARAS DE GIRASOL (Helianthus annus L .) COMO ENMIENDA ORGÁNICA Y SUS EFECTOS SOBRE PROPIEDADES DEL SUELO SUNFLOWER (Helianthus annus L .) HULL AS AN ORGANIC AMENDMENT AND ITS EFFECTS ON SOIL PROPERTIES, Agro-Ciencia. 28 (2012) 117–126.

[17] F.D. Castaño, The sunflower crop in Argentina: Past, present and potential Future, OCL - Oilseeds Fats, Crop. Lipids. (2018). https://doi.org/10.1051/ocl/2017043.

[18] J.H. Yuan, R.K. Xu, The amelioration effects of low temperature biochar generated from nine crop residues on an acidic Ultisol, Soil Use Manag. 27 (2011) 110–115. https://doi.org/10.1111/j.1475-2743.2010.00317.x.

[19] O. Kazak, A. Tor, In situ preparation of magnetic hydrochar by co-hydrothermal treatment of waste vinasse with red mud and its adsorption property for Pb(II) in aqueous solution, J. Hazard. Mater. 393 (2020) 122391. https://doi.org/10.1016/j.jhazmat.2020.122391.

[20] S. Guo, X. Dong, K. Liu, H. Yu, C. Zhu, Chemical, energetic, and structural characteristics of hydrothermal carbonization solid products for lawn grass,

BioResources. 10 (2015) 4613–4625. https://doi.org/10.15376/biores.10.3.4613-4625.

[21] M.A. Khan, A.A. Alqadami, M. Otero, M.R. Siddiqui, Z.A. Alothman, I. Alsohaimi, M. Rafatullah, A.E. Hamedelniel, Heteroatom-doped magnetic hydrochar to remove post-transition and transition metals from water: Synthesis, characterization, and adsorption studies, Chemosphere. 218 (2019) 1089–1099. https://doi.org/10.1016/j.chemosphere.2018.11.210.

[22] H. Sayğılı, Hydrothermal synthesis of magnetic nanocomposite from biowaste matrix by a green and one-step route: Characterization and pollutant removal ability, Bioresour. Technol. 278 (2019) 242–247. https://doi.org/10.1016/j.biortech.2019.01.103.

[23] A.L. Tasca, M. Puccini, R. Gori, I. Corsi, A.M.R. Galletti, S. Vitolo, Hydrothermal carbonization of sewage sludge: A critical analysis of process severity, hydrochar properties and environmental implications, Waste Manag. 93 (2019) 1–13. https://doi.org/10.1016/j.wasman.2019.05.027.

[24] J. Yu, Z. Zhu, H. Zhang, T. Chen, Y. Qiu, Z. Xu, D. Yin, Efficient removal of several estrogens in water by Fe-hydrochar composite and related interactive effect mechanism of H2O2 and iron with persistent free radicals from hydrochar of pinewood, Sci. Total Environ. 658 (2019) 1013–1022. https://doi.org/10.1016/j.scitotenv.2018.12.183.

[25] W. Wang, H. Wang, G. Li, P.K. Wong, T. An, Visible light activation of persulfate by magnetic hydrochar for bacterial inactivation: Efficiency, recyclability and mechanisms, Water Res. 176 (2020) 115746. https://doi.org/10.1016/j.watres.2020.115746.

[26] M.F. Horst, M. Alvarez, V.L. Lassalle, Removal of heavy metals from wastewater using magnetic nanocomposites: Analysis of the experimental conditions, Sep. Sci. Technol. 51 (2016) 550–563. https://doi.org/10.1080/01496395.2015.1086801.

[27] M.F. Horst, D.F. Coral, M.B. Fernández van Raap, M. Alvarez, V. Lassalle, Hybrid nanomaterials based on gum Arabic and magnetite for hyperthermia treatments, Mater. Sci. Eng. C. 74 (2016) 443–450. https://doi.org/10.1016/j.msec.2016.12.035.

[28] A. Šutka, S. Lagzdina, T. Käämbre, R. Pärna, V. Kisand, J. Kleperis, M. Maiorov, A. Kikas, I. Kuusik, D. Jakovlevs, Study of the structural phase transformation of iron oxide nanoparticles from an Fe2+ ion source by precipitation under various synthesis parameters and temperatures, Mater. Chem. Phys. (2015). https://doi.org/10.1016/j.matchemphys.2014.10.048.

[29] J. Rouquerol, G. Baron, R. Denoyel, H. Giesche, J. Groen, P. Klobes, P. Levitz, A. V Neimark, S. Rigby, R. Skudas, Recommendations for the characterization of porous solids (Technical Report), Pure Appl. Chem. 66 (1994) 1739–1758. https://doi.org/10.1351/pac199466081739.

[30] M.T. Reza, E. Rottler, R. Tölle, M. Werner, P. Ramm, J. Mumme, Production, characterization, and biogas application of magnetic hydrochar from cellulose, Bioresour. Technol. 186 (2015) 34–43. https://doi.org/10.1016/j.biortech.2015.03.044.

[31] T.H. Liou, Development of mesoporous structure and high adsorption capacity of biomass-based activated carbon by phosphoric acid and zinc chloride activation, Chem. Eng. J. 158 (2010) 129–142. https://doi.org/10.1016/j.cej.2009.12.016.

[32] A.A. Oladipo, A.O. Ifebajo, Highly efficient magnetic chicken bone biochar for removal of tetracycline and fluorescent dye from wastewater: Two-stage adsorber analysis, J. Environ. Manage. 209 (2018) 9–16. https://doi.org/10.1016/j.jenvman.2017.12.030.

[33] L. Zhang, S. Liu, B. Wang, Q. Wang, G. Yang, J. Chen, Effect of residence time on hydrothermal carbonization of corn cob residual, BioResources. 10 (2015) 3979–3986. https://doi.org/10.15376/biores.10.3.3979-3986.

[34] J.H. Yuan, R.K. Xu, H. Zhang, The forms of alkalis in the biochar produced from crop

residues at different temperatures, Bioresour. Technol. 102 (2011) 3488–3497. https://doi.org/10.1016/j.biortech.2010.11.018.

[35] A.J. Romero-Anaya, M. Ouzzine, M.A. Lillo-Ródenas, A. Linares-Solano, Spherical carbons: Synthesis, characterization and activation processes, Carbon N. Y. 68 (2014) 296–307. https://doi.org/10.1016/j.carbon.2013.11.006.

[36] I. Ali, M. Asim, T.A. Khan, Low cost adsorbents for the removal of organic pollutants from wastewater, J. Environ. Manage. 113 (2012) 170–183. https://doi.org/10.1016/j.jenvman.2012.08.028.

[37] E. Behazin, E. Ogunsona, A. Rodriguez-Uribe, A.K. Mohanty, M. Misra, A.O. Anyia, Mechanical, Chemical and Physical properties of wood and perennial grass biochars for possible composite application, BioResources. 11 (2016) 1334–1348.

[38] S. Nizamuddin, N.S. Jaya Kumar, J.N. Sahu, P. Ganesan, N.M. Mubarak, S.A. Mazari, Synthesis and characterization of hydrochars produced by hydrothermal carbonization of oil palm shell, Can. J. Chem. Eng. 93 (2015) 1916–1921. https://doi.org/10.1002/cjce.22293.

[39] X. Zhu, Y. Liu, F. Qian, C. Zhou, S. Zhang, J. Chen, Role of Hydrochar Properties on the Porosity of Hydrochar-based Porous Carbon for Their Sustainable Application, ACS Sustain. Chem. Eng. (2015). https://doi.org/10.1021/acssuschemeng.5b00153.

[40] M. Keiluweit, P.S. Nico, M.G. Johnson, M. KLEBER, Dynamic Molecular Structure of Plant Biomass-derived Black Carbon(Biochar)- Supporting Information -, Environ. Sci. Technol. 44 (2010) 1247–1253. 10.1021/es9031419.

[41] A. Shaaban, S.M. Se, N.M.M. Mitan, M.F. Dimin, Characterization of biochar derived from rubber wood sawdust through slow pyrolysis on surface porosities and functional groups, Procedia Eng. 68 (2013) 365–371. https://doi.org/10.1016/j.proeng.2013.12.193.

[42] X. Zhu, Y. Liu, F. Qian, C. Zhou, S. Zhang, J. Chen, Preparation of magnetic porous carbon from waste hydrochar by simultaneous activation and magnetization for tetracycline removal, Bioresour. Technol. 154 (2014) 209–214. https://doi.org/10.1016/j.biortech.2013.12.019.

[43] B. Armynah, Atika, Z. Djafar, W.H. Piarah, D. Tahir, Analysis of Chemical and Physical Properties of Biochar from Rice Husk Biomass, J. Phys. Conf. Ser. 979 (2018). https://doi.org/10.1088/1742-6596/979/1/012038.

[44] R. Onyenwoke, J. Wiegel, Magnetite : Structure , Properties and Applications, (2014).

[45] F. Quesada-Plata, R. Ruiz-Rosas, E. Morallón, D. Cazorla-Amorós, Activated Carbons Prepared through H3PO4-Assisted Hydrothermal Carbonisation from Biomass Wastes: Porous Texture and Electrochemical Performance, Chempluschem. 81 (2016) 1349–1359. https://doi.org/10.1002/cplu.201600412.

[46] C. Di Dong, C.W. Chen, C.M. Kao, C.C. Chien, C.M. Hung, Wood-biochar-supported magnetite nanoparticles for remediation of PAH-contaminated estuary sediment, Catalysts. 8 (2018) 1–13. https://doi.org/10.3390/catal8020073.

[47] D. Mohan, H. Kumar, A. Sarswat, M. Alexandre-Franco, C.U. Pittman, Cadmium and lead remediation using magnetic oak wood and oak bark fast pyrolysis bio-chars, Chem. Eng. J. 236 (2014) 513–528. https://doi.org/10.1016/j.cej.2013.09.057.

[48] X. Li, C. Wang, J. Zhang, J. Liu, B. Liu, G. Chen, Preparation and application of magnetic biochar in water treatment: A critical review, Sci. Total Environ. 711 (2020) 134847. https://doi.org/10.1016/j.scitotenv.2019.134847.

[49] S. Vahdati-Khajeh, M. Zirak, R.Z. Tejrag, A. Fathi, K. Lamei, B. Eftekhari-Sis, Biocompatible magnetic N-rich activated carbon from egg white biomass and sucrose: Preparation, characterization and investigation of dye adsorption capacity from aqueous

solution, Surfaces and Interfaces. 15 (2019) 157–165. https://doi.org/10.1016/j.surfin.2019.03.003.

[50] X. Zhu, F. Qian, Y. Liu, S. Zhang, J. Chen, Environmental performances of hydrochar-derived magnetic carbon composite affected by its carbonaceous precursor, RSC Adv. 5 (2015) 60713–60722. https://doi.org/10.1039/c5ra07339a.

[51] P. Nicolás, M. Saleta, H. Troiani, R. Zysler, V. Lassalle, M.L. Ferreira, Preparation of iron oxide nanoparticles stabilized with biomolecules: Experimental and mechanistic issues, Acta Biomater. 9 (2013) 4754–4762. https://doi.org/10.1016/j.actbio.2012.09.040.

[52] F.N. Çatlıoğlu, S. Akay, B. Gözmen, E. Turunc, I. Anastopoulos, B. Kayan, D. Kalderis, Fe-modified hydrochar from orange peel as adsorbent of food colorant Brilliant Black: process optimization and kinetic studies, Int. J. Environ. Sci. Technol. 17 (2020) 1975–1990. https://doi.org/10.1007/s13762-019-02593-z.

[53] E. Vunain, D. Kenneth, T. Biswick, Synthesis and characterization of low-cost activated carbon prepared from Malawian baobab fruit shells by H3PO4 activation for removal of Cu(II) ions: equilibrium and kinetics studies, Appl. Water Sci. 7 (2017) 4301–4319. https://doi.org/10.1007/s13201-017-0573-x.

[54] X. Wang, J. Xu, J. Liu, J. Liu, F. Xia, C. Wang, R.A. Dahlgren, W. Liu, Mechanism of Cr(VI) removal by magnetic greigite/biochar composites, Sci. Total Environ. 700 (2020) 134414. https://doi.org/10.1016/j.scitotenv.2019.134414.

[55] Y. Li, A.R. Zimmerman, F. He, J. Chen, L. Han, H. Chen, X. Hu, B. Gao, Solvent-free synthesis of magnetic biochar and activated carbon through ball-mill extrusion with Fe3O4 nanoparticles for enhancing adsorption of methylene blue, Sci. Total Environ. 722 (2020) 137972. https://doi.org/10.1016/j.scitotenv.2020.137972.

[56] N. Van Vinh, M. Zafar, S.K. Behera, H.S. Park, Arsenic(III) removal from aqueous solution by raw and zinc-loaded pine cone biochar: equilibrium, kinetics, and thermodynamics studies, Int. J. Environ. Sci. Technol. 12 (2015) 1283–1294. https://doi.org/10.1007/s13762-014-0507-1.

[57] Ç. Şentorun-Shalaby, M.G. Uçak-Astarlioğlu, L. Artok, Ç. Sarici, Preparation and characterization of activated carbons by one-step steam pyrolysis/activation from apricot stones, Microporous Mesoporous Mater. 88 (2006) 126–134. https://doi.org/10.1016/j.micromeso.2005.09.003.

[58] O. Duman, S. Tunç, T.G. Polat, B.K.I. Bozoğlan, Synthesis of magnetic oxidized multiwalled carbon nanotube-κ-carrageenan-Fe3O4 nanocomposite adsorbent and its application in cationic Methylene Blue dye adsorption, Carbohydr. Polym. 147 (2016) 79–88. https://doi.org/10.1016/j.carbpol.2016.03.099.

[59] S. Cheng, L. Zhang, H. Xia, J. Peng, J. Shu, C. Li, Ultrasound and microwave-assisted preparation of Fe-activated carbon as an effective low-cost adsorbent for dyes wastewater treatment, RSC Adv. 6 (2016) 78936–78946. https://doi.org/10.1039/c6ra14082c.

[60] O. Kazak, Y.R. Eker, H. Bingol, A. Tor, Preparation of chemically-activated high surface area carbon from waste vinasse and its efficiency as adsorbent material, J. Mol. Liq. 272 (2018) 189–197. https://doi.org/10.1016/j.molliq.2018.09.085.

[61] S. Takami, T. Sato, T. Mousavand, S. Ohara, M. Umetsu, T. Adschiri, Hydrothermal synthesis of surface-modified iron oxide nanoparticles, Mater. Lett. 61 (2007) 4769–4772. https://doi.org/10.1016/j.matlet.2007.03.024.

[62] T. Dittmar, C.E. De Rezende, M. Manecki, J. Niggemann, A.R. Coelho Ovalle, A. Stubbins, M.C. Bernardes, Continuous flux of dissolved black carbon from a vanished tropical forest biome, Nat. Geosci. (2012). https://doi.org/10.1038/ngeo1541.

[63] C.H. Liu, W. Chu, H. Li, S.A. Boyd, B.J. Teppen, J. Mao, J. Lehmann, W. Zhang, Quantification and characterization of dissolved organic carbon from biochars, Geoderma. 335 (2019) 161–169. https://doi.org/10.1016/j.geoderma.2018.08.019.

[64] C.R. Smith, P.G. Hatcher, S. Kumar, J.W. Lee, Investigation into the Sources of Biochar Water-Soluble Organic Compounds and Their Potential Toxicity on Aquatic Microorganisms, ACS Sustain. Chem. Eng. (2016). https://doi.org/10.1021/acssuschemeng.5b01687.

[65] X. Qu, H. Fu, J. Mao, Y. Ran, D. Zhang, D. Zhu, Chemical and structural properties of dissolved black carbon released from biochars, Carbon N. Y. (2016). https://doi.org/10.1016/j.carbon.2015.09.106.

[66] V.L. Lassalle, R.D. Zysler, M.L. Ferreira, Novel and facile synthesis of magnetic composites by a modified co-precipitation method, Mater. Chem. Phys. 130 (2011) 624–634. https://doi.org/10.1016/j.matchemphys.2011.07.035.

Captions of Figures and Tables

Scheme 1. Graphical view of the pathways for the experimental procedure. (the authors acknowledge the contribution of **Mind the graph**)

Figure 1. FTIR spectra of SFH and HC

Figure 2. FTIR spectra of HC and MHC

Figure 3. X-ray diffraction patterns of MHC and HC

Figure 4. TEM images of a) HC, b) neck magnetite, c and d) MHC

Figure 5. Magnetization curve at room temperature for MHC

Figure 6. Z potential as function of pH of HC, MHC and naked magnetite in different electrolytes: a) 0.001 M KNO_3 (HC and MHC initial pH :4.79 and 6.41)

b) 0.001 M NaCl (HC and MHC initial pH :5.55 and 5.36) and

Figure 7. Weight loss as function of temperature for MHC and HC

Figure 8. Stability assays a) in bidistilled water and b) real water sample

Figure 9. Mechanism proposed for hydrochar and magnetite nanoparticles linkage

Table 1. Chemical composition of hydrochars and sunflower husk

Table 2. Hydrodynamic diameter, PDI and Z potential of hydrochars and sunflower husk

Table 3. Surface area and porous structures for SFH and hydrochars

Table 1. Chemical composition of hydrochars and sunflower husk

Sample	Residence time (horas)							
		Yield%	%C	%H	%N	%O*	H/C	O/C
HC1	3	47	67.02	5.41	0.45	27.12	0.080	0.405
HC2	6	45	67.72	5.31	0.35	26.62	0.078	0.393
HC3	24	43	68.40	4.81	0.34	26.45	0.070	0.386
SFH			46.57	6.32	0.96	46.15	0.14	0.990

Table 2. Hydrodynamic diameter, PDI and Z potential of hydrochars and sunflower husk

Sample	H_D (nm)	PDI	*Zpot (mV)
SFH	876.55	0.823	-11.15
HC1	1728.25	0.586	-6.16
HC2	1260.5	0.548	-6.65
HC3	779.125	0.333	-8.28
Mag	532.56	0.386	-7.51
MHC	670.73	0.431	-20.3

*No ionic strength adjusted (pH= 5.5)

Table 3. Surface area and porous structures for SFH and hydrochars

Sample	Residence time (horas)	BET Surface area (m^2/g)	Pore volume (cm^3/g)	Pore width (nm)
HC1	3	150	0,19	2,49
HC2	6	39,16	0,0739	2,79
HC3	24	22,46	0,0276	2,77
SFH		23,14	0,0206	0,924